Analytical Steady-State Solution to the Rapid Buffering Approximation Near an Open Ca^{2+} Channel

Gregory D. Smith
Institute of Theoretical Dynamics, Biophysics Graduate Group, University of California, Davis, California 95616

ABSTRACT We derive an analytical steady-state solution for the Ca^{2+} profile near an open Ca^{2+} channel based on a transport equation which describes the buffered diffusion of Ca^{2+} in the presence of rapid stationary and mobile Ca^{2+} buffers (Wagner and Keizer, 1994). This steady-state rapid buffering approximation gives an upper bound on local Ca^{2+} elevations such as Ca^{2+} puffs or sparks when conditions for the validity of the rapid buffering approximation are met and is an alternative to approximations that assume that mobile buffers are unsaturable. This result also provides an analytical estimate of the cytosolic Ca^{2+} domain concentration ($[Ca^{2+}]_d$) near a channel pore and shows the dependence of $[Ca^{2+}]_d$ on moderate concentrations of endogenous mobile buffer, Ca^{2+} indicator dye, and bulk cytosolic Ca^{2+}. Assuming a simple relationship between $[Ca^{2+}]_d$ and the lumenal depletion domain of an intracellular Ca^{2+} channel, lumenal and cytosolic Ca^{2+} profiles are matched to give an implicit analytical expression for the effect of bulk lumenal Ca^{2+} on $[Ca^{2+}]_d$.

INTRODUCTION

Localized elevations of intracellular free Ca^{2+} because of release from intracellular Ca^{2+} stores and Ca^{2+} influx across the plasma membrane are observed in various cell types using confocal microscopy. In the immature *Xenopus laevis* oocyte, intracellular Ca^{2+} release events dubbed "Ca^{2+} puffs" occur in response to flash photolysis of caged inositol trisphosphate (IP_3) and microinjection of a nonhydrolyzable IP_3 analog (Yao et al., 1995; Parker and Yao, 1996). In cardiac myocytes, spontaneous Ca^{2+} elevations observed under both normal and Ca^{2+}-overload conditions appear to be the result of the opening of single sarcoplasmic Ca^{2+} release channels (Cheng et al., 1993). These ryanodine receptor-mediated "Ca^{2+} sparks" can also be evoked in response to Ca^{2+} influx activated by membrane depolarization (Cannell et al., 1995). Whereas increases in bulk Ca^{2+} initiate contraction of arterial smooth muscle, Ca^{2+} sparks induce relaxation through the local activation of Ca^{2+}-activated potassium channels (Nelson et al., 1995). In chromaffin cells, pulsed laser imaging detects short-lived Ca^{2+} gradients due to voltage-gated Ca^{2+} entry (Monck et al., 1994). "Hot spots" associated with Ca^{2+} influx near synaptic release sites in the base of turtle hair cells are observed during membrane depolarization (Tucker and Fettiplace, 1995). Ca^{2+} hot spots are also observed during electrical stimulation of neuroblastoma cells in which Ca^{2+} influx through clusters of L-type Ca^{2+} channels modulates growth cone behavior (Silver et al., 1990). These and other reports suggest that localized Ca^{2+} elevations are an important aspect of Ca^{2+} signaling (Rizzuto et al., 1993; Clapham, 1995).

Local Ca^{2+} elevations participate in Ca^{2+} signaling by regulating Ca^{2+}-gated plasma membrane ion channels. Voltage-gated Ca^{2+} channels in the pancreatic β-cell, for example, are inactivated by domain Ca^{2+} (Sherman et al., 1990). Local Ca^{2+} elevations activate potassium channels in saccular hair cells (Roberts, 1993), pituitary gonadotrophs (Li et al., 1995), and arterial smooth muscle (Nelson et al., 1995). They are also relevant to stimulus-secretion coupling in chromaffin cells (Zhou and Neher, 1993; Heinemann et al., 1994) and the squid giant synapse (Zucker and Fogelson, 1986; Adler et al., 1991). Density-dependent cooperativity of Ca^{2+}- and Ba^{2+}-mediated inactivation of L-type Ca^{2+} channels in embryonic chick ventricle cells suggests that under physiological conditions, clusters of voltage-gated Ca^{2+} channels share domain Ca^{2+} (Mazzanti et al., 1991; Risso and DeFelice, 1993; DeFelice, 1993). For a plasma membrane Ca^{2+} channel, the domain Ca^{2+} concentration ($[Ca^{2+}]_d$) is a function of the single-channel current and is largely determined by the membrane potential and external Ca^{2+} concentration (Sherman et al., 1990).

Local Ca^{2+} signals also regulate Ca^{2+} release from intracellular stores. The local activation of ryanodine receptors (RyRs) by Ca^{2+} influx through single dihydropyridine receptors is a fundamental event in excitation-contraction coupling of cardiac myocytes (Cannell et al., 1994). Ca^{2+} puffs may be attributable to local regenerative Ca^{2+} release from clusters of IP_3-receptor/Ca^{2+} channels (IP_3Rs) followed by Ca^{2+}-inactivation (Yao et al., 1995; Bezprozvanny and Ehrlich, 1995; Parker and Yao, 1996). In the case of intracellular Ca^{2+} channels, $[Ca^{2+}]_d$ may be largely determined by the lumenal Ca^{2+} concentration (Swillens et al., 1994; Horne and Meyer, 1995). Indeed, recent planar lipid bilayer experiments suggest that both the IP_3R and the RyR are indirectly regulated by lumenal Ca^{2+} via the action of domain Ca^{2+} upon a cytosolic binding site (Bezprozvanny and Ehrlich, 1994; Tripathy and Meissner, 1996).

Received for publication 1 August 1996 and in final form 19 September 1996.

Address reprint requests to Gregory D. Smith, Institute of Theoretical Dynamics, 2201 Academic Surge Bldg., University of California, Davis, CA 95616. Tel.: 916-752-8275; Fax: 916-752-7297; E-mail: smith@itd.ucdavis.edu.

0006-3495/96/12/3064/09 $2.00

Another aspect of Ca^{2+} signaling that affects Ca^{2+} microdomains is the association of Ca^{2+} with cytosolic Ca^{2+}-binding proteins. Cellular Ca^{2+} buffers, whether stationary or mobile, reduce the basal free Ca^{2+} concentration and localize Ca^{2+} signals by reducing the effective diffusion coefficient for Ca^{2+} (Allbritton et al., 1992). Mobile Ca^{2+} buffers have an additional "sink" effect on free Ca^{2+} in proportion to the local Ca^{2+} gradient that both restricts Ca^{2+} elevations and facilitates Ca^{2+} clearance after channel inactivation. Ca^{2+} indicator dyes are themselves mobile Ca^{2+} buffers and perturb local Ca^{2+} elevations (Wagner and Keizer, 1994; Smith et al., 1996). For all these reasons, theoretical treatments of Ca^{2+} microdomains should include mobile buffers. The following section reviews several mathematical equations used in the analysis of Ca^{2+} microdomains.

MATHEMATICAL BACKGROUND

Calculations of local Ca^{2+} elevations that include mobile buffers involve the numerical solution of a set of reaction-diffusion equations of the following form (Stern, 1992; Wagner and Keizer, 1994),

$$\frac{\partial[Ca^{2+}]}{\partial t} = D_c\nabla^2[Ca^{2+}] + \sum_j R_j + \sigma\delta(r) \quad (1)$$

$$\frac{\partial[B_j]}{\partial t} = D_j\nabla^2[B_j] + R_j. \quad (2)$$

Assuming independent bimolecular association reactions between Ca^{2+} and buffer, the R_j are given by

$$R_j = -k_j^+[B_j][Ca^{2+}] + k_j^-([B_j]_T - [B_j]). \quad (3)$$

In these equations, the full equations for the buffered diffusion of Ca^{2+}, j is an index over each buffer; $[B_j]_T$ and D_j are the total concentration and diffusion constant of buffer j; k_j^+ and k_j^- are association and dissociation rate constants; D_c is the diffusion constant of free Ca^{2+}; and $\delta(r)$, the Dirac delta function, is a sharply peaked function at the origin. The concentration profiles of Ca^{2+}-bound buffer are given by $[CaB_j] = [B_j]_T - [B_j]$, provided that the diffusion constant of each buffer is not affected by the binding of Ca^{2+} and that the initial concentration profile of each buffer is uniform (Wagner and Keizer, 1994). These full equations for the buffered diffusion of Ca^{2+} have been used to analyze the ability of fast (BAPTA) and slow (EGTA) Ca^{2+} chelators to buffer Ca^{2+} in the vicinity of a channel pore (Stern, 1992). Both time-dependent and steady-state versions of the full equations have been numerically solved to simulate Ca^{2+} buffering by Calbindin-D_{28K} in the saccular hair cell (Roberts, 1994). However, the implementation of such calculations can be time-consuming.

An analytical solution to the full equations derived by Neher (1986) is an alternative to this computational approach. This analytical approximation to the steady-state Ca^{2+} profile near a Ca^{2+} channel begins with a time-independent version of Eqs. 1–3 and assumes that mobile buffers are unsaturable. In the case of a single such mobile buffer, this assumption ($[B_m] \approx [B_m]_T$, $[B_m]$, and $[CaB_m]$ assumed constant in space and time) can be used to write (Neher, 1986)

$$\frac{\partial[Ca^{2+}]}{\partial t} = D_c\nabla^2[Ca^{2+}] - k_m^+[B_m]_T([Ca^{2+}] - c_\infty) + \sigma\delta(r), \quad (4)$$

where c_∞ is the bulk Ca^{2+} concentration far from the channel. A steady state to Eq. 4 is given by (see Appendix A)

$$[Ca^{2+}] = \frac{\sigma}{2\pi D_c r}e^{-r/\lambda} + c_\infty \quad (5)$$

where the characteristic length (λ) for the mobile Ca^{2+} buffer is $\lambda = \sqrt{D_c/k_m^+[B_m]_T}$. This equation, called the excess buffer approximation, can be used when the saturability of mobile Ca^{2+} buffer is negligible. For example, the presence of millimolar Calbindin-D_{28K} in the saccular hair cell allows its use (Roberts, 1993). This assumption is also appropriate when cells are dialyzed with high concentrations of exogenous Ca^{2+} chelator (Zweifach and Lewis, 1995). However, in the case of intracellular Ca^{2+} release events such as puffs and sparks, mobile Ca^{2+} buffer is present in moderate, saturable concentrations. The excess buffer approximation cannot be used to analyze these localized Ca^{2+} elevations.

Whereas the excess buffer approximation is generally not valid in the case of Ca^{2+} puffs and sparks, in some cases the rapid buffering approximation is applicable (Smith et al., 1996). When the kinetics of Ca^{2+} buffers are fast compared to the diffusive time scale, the rapid buffering approximation can be used to reduce the full equations to the following form (Wagner and Keizer, 1994),

$$\frac{\partial[Ca^{2+}]}{\partial t} = \beta\left[\left(D_c + \sum_j \gamma_j D_j\right)\nabla^2[Ca^{2+}] - 2\left(\sum_j \frac{\gamma_j D_j}{K_j + [Ca^{2+}]}\right)\nabla[Ca^{2+}]\cdot\nabla[Ca^{2+}] + \sigma\delta(r)\right], \quad (6)$$

where $\beta = (1 + \Sigma_j \gamma_j)^{-1}$, $\gamma_j = K_j[B_j]_T/(K_j + [Ca^{2+}])^2$, and K_j, the dissociation constant of buffer j, is given by $K_j = k_j^-/k_j^+$. See Wagner and Keizer, 1994, for the derivation of this reduced equation for the buffered diffusion of Ca^{2+} and a precise statement of how the validity of the rapid buffering approximation near an open Ca^{2+} channel depends on buffer equilibration times, unitary current, and total mobile buffer concentration.

In the following section, we derive a novel analytical approximation to the steady-state Ca^{2+} profile near a Ca^{2+} channel that begins with this reduced equation for the buffered diffusion of Ca^{2+}. Because the reduced equation does not assume that mobile buffers are unsaturable, this steady-state rapid buffering approximation is valid in some situations where the excess buffer approximation is not applica

ble; and it is an alternative to the excess buffer approximation that can be used to analyze 1) the source amplitude of local Ca^{2+} elevations such as Ca^{2+} puffs and sparks, 2) the effect of moderate concentrations of mobile buffer on the Ca^{2+} domain concentration ($[Ca^{2+}]_d$) near a channel pore, and 3) the dependence of $[Ca^{2+}]_d$ near an intracellular Ca^{2+} channel on bulk lumenal Ca^{2+}.

Steady-state rapid buffering approximation near an open Ca^{2+} channel

Setting $\partial[Ca^{2+}]/\partial t = 0$ in Eq. 6 and using hemispherical symmetry to rewrite the Laplacian and gradient leads to the following ordinary differential equation for the steady-state Ca^{2+} profile near a Ca^{2+} channel,

$$\frac{d^2[Ca^{2+}]}{dr^2} = -\frac{2}{r}\frac{d[Ca^{2+}]}{dr} + f([Ca^{2+}])\left(\frac{d[Ca^{2+}]}{dr}\right)^2 \quad (r > 0) \tag{7}$$

where the function $f([Ca^{2+}])$ is defined by

$$f([Ca^{2+}]) \equiv 2\left(\sum_j \frac{\gamma_j D_j}{K_j + [Ca^{2+}]}\right) \Big/ \left(D_c + \sum_j \gamma_j D_j\right). \tag{8}$$

An implicit analytical solution to this ordinary differential equation (see Appendix B) is given by

$$D_c[Ca^{2+}] - \sum_j \frac{\Phi_j}{K_j + [Ca^{2+}]} = -\frac{C_1}{r} + C_2 \tag{9}$$

where $\Phi_j = D_j[B_j]_T K_j$ and the constants C_1 and C_2 are determined by the boundary conditions. If the source amplitude (σ) of the Ca^{2+} channel and the bulk Ca^{2+} concentration (c_∞) far from the channel are used to specify C_1 and C_2 (see Appendix B), Eq. 9 becomes,

$$D_c[Ca^{2+}] - \sum_j \frac{\Phi_j}{K_j + [Ca^{2+}]} = \frac{\sigma}{2\pi r} + D_c c_\infty - \sum_j \frac{\Phi_j}{K_j + c_\infty}, \tag{10}$$

where the 2π signifies hemispherical symmetry (Stern, 1992). In the case of one mobile buffer (at concentration $[B_m]_T$ with affinity K_m and mobility D_m), Eq. 10 is a quadratic equation that can be solved to give

$$[Ca^{2+}] = \left(-D_c K_m + \frac{\sigma}{2\pi r} + C_2 + \sqrt{\left(D_c K_m + \frac{\sigma}{2\pi r} + C_2\right)^2 + 4D_c\Phi_m}\right)/2D_c \tag{11}$$

where

$$C_2 = D_c c_\infty - \frac{\Phi_m}{K_m + c_\infty} \tag{12}$$

and $\Phi_m = D_m[B_m]_T K_m$ (see Appendix B). Note that when no mobile buffer is present Eq. 11 reduces to $[Ca^{2+}] = \sigma/2\pi D_c r + c_\infty$, which is the steady-state solution of Eq. 4 when $[B_m]_T = 0$.

This derivation of the steady-state rapid buffering approximation is confirmed in Fig. 1, where the steady-state Ca^{2+} profile given by Eq. 11 is compared to a time-dependent numerical solution of Eq. 6. For parameters chosen to represent a single Ca^{2+} channel (σ = 0.5 pA) in the presence of one stationary ($[B_s]_T$ = 250 μM, K_s = 1 μM) and one mobile ($[B_m]_T$ = 50 μM, K_m = 1 μM) buffer, the analytical steady-state rapid buffering approximation is indeed the limit of the time-dependent numerical solution as time elapses, and this convergence is extremely rapid near the source (Simon and Llinás, 1985). Fig. 1 also shows that Eq. 11 provides an extremely good approximation to the Ca^{2+} domain concentration ($[Ca^{2+}]_d$) near the channel. Because moderate concentrations of mobile Ca^{2+} buffer are present, the excess buffer approximation cannot be used to estimate this steady-state Ca^{2+} profile, and simply ignoring mobile buffer leads to a gross overestimate of this microdomain.

Estimating source amplitude from Ca^{2+}-bound dye profiles

The steady-state rapid buffering approximation can be used to estimate the source amplitude of local Ca^{2+} elevations that occur in the presence of several mobile Ca^{2+} buffers. For example, assuming a source amplitude of 5 pA, 50 μM endogenous mobile Ca^{2+} buffer (K_m = 1 μM, D_m = 75 $\mu m^2/s$), and 40 μM exogenous Ca^{2+}-indicator dye (K_e = 0.25 μM, D_e = 75 $\mu m^2/s$), the steady-state Ca^{2+} profile (*solid line*) in Fig. 2 *A* was easily calculated using a program

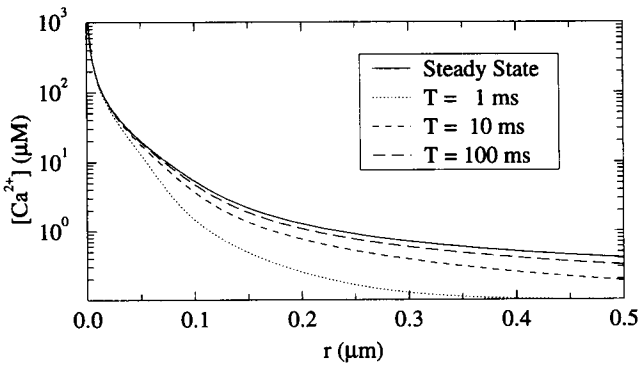

FIGURE 1 Steady-state analytical calculation of the Ca^{2+} profile (*solid line*) near an open Ca^{2+} channel given by Eq. 11 is compared to time-dependent solutions of the rapid buffering approximation (*broken lines*) shown at 1, 10, and 100 ms. Parameters: $[B_s]_T$ = 250 μM, $[B_m]_T$ = 50 μM, $K_s = K_m$ = 1 μM, D_c = 250 $\mu m^2/s$, D_m = 75 $\mu m^2/s$, c_∞ = 0.1 μM, and σ = 0.5 pA. Here and in the figures to follow, σ is converted into units of μmol/s using Faraday's constant before substitution into Eq. 11, the units of which are then reconciled by noting that 1 L is 10^{15} μm^3. In the time-dependent calculation, Δt = 0.1 ms, Δr ranged from 0.001 μm to 1 μm, and an absorbing boundary condition was imposed at $r \approx 30$ μm. The numerical method used has been previously described (Smith et al., 1996). Note that the analytical steady-state result is the limit of the time-dependent result as time elapses, and this convergence is rapid near the source.

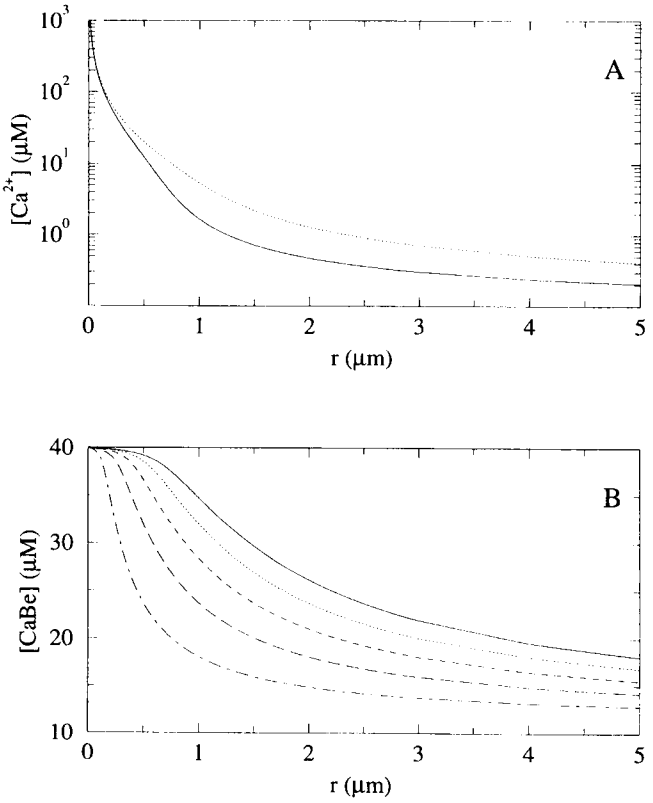

FIGURE 2 Steady-state Ca^{2+} and Ca^{2+}-bound dye (CaB_e) profiles calculated using a program that numerically solves for the roots of Eq. 10. The source amplitude (σ = 5 pA) corresponds to a local Ca^{2+} elevation such as a Ca^{2+} puff or spark. (*A*) Estimated steady-state Ca^{2+} profile (*solid line*) when both endogenous Ca^{2+} buffer ($[B_m]_T$ = 50 μM, K_m = 1 μM, D_m = 75 $\mu m^2/s$) and exogenous Ca^{2+}-indicator dye ($[B_e]_T$ = 40 μM, K_e = 0.25 μM, D_e = 75 $\mu m^2/s$) are included. The dotted line is the Ca^{2+} profile in the absence of indicator dye. Other parameters: D_c = 250 $\mu m^2/s$, c_∞ = 0.1 μM. (*B*) Solid line is the steady-state Ca^{2+}-bound indicator dye profile corresponding to the 5 pA source used above. Broken lines show steady-state CaB_e profile predicted for σ = 4, 3, 2, and 1 pA.

that numerically solves for the roots of Eq. 10 for each radius (r) of interest. The solid line in Fig. 2 *B* shows the steady-state Ca^{2+}-bound indicator dye (CaB_e) profile, given by $[CaB_e] = [B_e]_T[Ca^{2+}]/(K_e + [Ca^{2+}])$. The steady-state rapid buffering approximation can also be used to estimate how much larger the Ca^{2+} profile would be if the indicator dye were not included (see Fig. 2 *A*, *dotted line*). The broken lines in Fig. 2 *B* show the CaB_e profiles predicted by the steady-state rapid buffering approximation for various source amplitudes (σ = 4, 3, 2, and 1 pA). Such steady-state Ca^{2+}-bound indicator dye profiles are easily calculated using Eq. 10 for any physiologically relevant panel of mobile Ca^{2+} buffers and can be used to estimate a minimum source amplitude for a given elevation in CaB_e.

Effect of rapid mobile buffer and bulk cytosolic Ca^{2+} on $[Ca^{2+}]_d$

Because the steady-state rapid buffering approximation is an analytical result, the relationship between various parameters is easily explored. For example, the effect of a single mobile buffer on $[Ca^{2+}]_d$ can be analyzed by fixing r in Eq. 10. This method is used in Fig. 3 (r = 0.03 μm) to plot $[Ca^{2+}]_d$ as a function of source amplitude (σ) for various mobile buffer parameters. The solid line in Fig. 3, *A* and *B* gives $[Ca^{2+}]_d$ in the absence of mobile buffer. Regardless of mobile buffer concentration or affinity, $[Ca^{2+}]_d$ is linearly proportional to the source amplitude (σ) when σ is large and, of course, $[Ca^{2+}]_d$ approaches the background Ca^{2+} concentration (c_∞ = 0.1 μM) when σ is small. The broken lines in Fig. 3 *A* show that moderate concentrations of rapid mobile buffer can significantly lower $[Ca^{2+}]_d$ for intermediate source amplitudes. Fig. 3 *B* shows that increasing the affinity of the buffer decreases $[Ca^{2+}]_d$, though higher affinity buffers are more easily saturated as σ is increased.

Another parameter that can affect $[Ca^{2+}]_d$ is the bulk cytosolic Ca^{2+} concentration (c_∞), which appears linearly in the excess buffer approximation but nonlinearly in the steady-state rapid buffering approximation. Using various mobile buffer parameters, Table 1 estimates the increase in

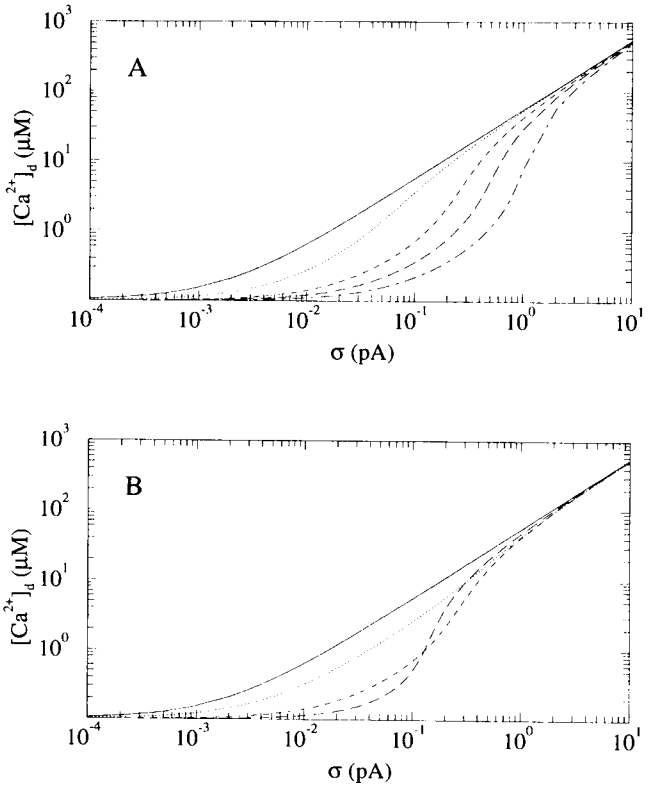

FIGURE 3 $[Ca^{2+}]_d$, defined as the Ca^{2+} concentration at r = 0.03 μm, is plotted as a function of source amplitude (σ) using the steady-state rapid buffering approximation, Eq. 11. The solid line gives $[Ca^{2+}]_d$ in absence of rapid mobile buffer ($[B_m]_T$ = 0 μM). (*A*) Effect of different total mobile buffer concentrations ($[B_m]_T$) on $[Ca^{2+}]_d$. Broken lines (from top to bottom) show $[Ca^{2+}]_d$ as a function of σ when $[B_m]_T$ takes values of 50, 100, and 200 μM. In all cases K_m = 1 μM, D_m = 75 $\mu m^2/s$, c_∞ = 0.1 μM, D_c = 250 $\mu m^2/s$. (*B*) Effect of rapid mobile buffer dissociation constant (K_m) on $[Ca^{2+}]_d$. Broken lines show $[Ca^{2+}]_d$ as a function of σ when K_m takes values of 10 (*dotted line*), 1.0 (*short-dashed line*), and 0.1 μM (*long-dashed line*). In all cases $[B_m]_T$ = 50 μM. Other parameters the same as in *A*.

TABLE 1 Effect of bulk cytosolic Ca^{2+} on $[Ca^{2+}]_d$

K_m (μM):	0.1	1.0	10
$[B_m]_T$ (μM)	$[Ca^{2+}]_d$ (μM): c_∞ = 0.1/1.0 μM		
50	47.6/54.7	41.8/48.8	43.1/45.1
100	40.2/53.3	28.8/41.7	32.5/35.3
150	32.7/52.0	16.7/34.7	23.8/27.2
200	25.3/50.7	7.6/28.1	17.5/20.9

The effect of bulk cytosolic Ca^{2+} concentration (c_∞) on $[Ca^{2+}]_d$ near a 0.5 pA Ca^{2+} channel estimated using Eq. 11 for a variety of buffer concentrations ($[B_m]_T$ = 50, 100, 150, 200 μM) and buffer affinities (K_m = 0.1, 1.0, 10 μM). $[Ca^{2+}]_d$ is calculated twice: first with c_∞ = 0.1 μM, then with c_∞ = 1.0 μM. A small increase in c_∞ often leads to a large increase in $[Ca^{2+}]_d$. Parameters: r = 0.03 μm, D_m = 75 $\mu m^2/s$, D_c = 250 $\mu m^2/s$.

$[Ca^{2+}]_d$ (σ = 0.5 pA, r = 0.03 μm) predicted by Eq. 11 when bulk Ca^{2+} rises from c_∞ = 0.1 μM to c_∞ = 1.0 μM. In the absence of mobile buffer, such an increase has only a minor effect: $[Ca^{2+}]_d$ increases from 55.1 μM to 56.0 μM. In the presence of mobile buffer, however, $[Ca^{2+}]_d$ can vary significantly as a function of bulk Ca^{2+}; e.g., with 100 μM mobile buffer (D_m = 75 $\mu m^2/s$, K_m = 0.1 μM), $[Ca^{2+}]_d$ increases by 12.9 μM as the bulk Ca^{2+} concentration rises from 0.1 μM to 1.0 μM. This dependence of $[Ca^{2+}]_d$ on bulk cytosolic Ca^{2+} is due to the saturability of mobile buffers and can be quantified using the steady-state rapid buffering approximation, but not the excess buffer approximation.

Near source estimate of the effect of rapid mobile buffer on $[Ca^{2+}]_d$

Although Eq. 10 provides an estimate of $[Ca^{2+}]_d$ in the presence of moderate concentrations or rapid mobile Ca^{2+} buffer, an even simpler expression for $[Ca^{2+}]_d$ can be derived by considering the limit of Eq. 11 as r goes to zero. When σ is positive and r is small, $[Ca^{2+}]_d$ is approximated by

$$[Ca^{2+}]_d^{app} \approx \left(-D_c K_m + \frac{\sigma}{2\pi r} + C_2 + \left|D_c K_m + \frac{\sigma}{2\pi r} + C_2\right|\right)\Big/ 2D_c. \quad (13)$$

Because the expression within the absolute value signs is greater than zero, this can be rewritten as

$$[Ca^{2+}]_d^{app} \approx \frac{\sigma}{2\pi D_c r} + c_\infty + \Delta[Ca^{2+}]_d^{app} \quad (14)$$

where $\Delta[Ca^{2+}]_d^{app}$, the difference between the steady-state rapid buffering approximation and the excess buffer approximation (Eq. 5) in the limit of small r, is given by

$$\Delta[Ca^{2+}]_d^{app} \equiv -\frac{\Phi_m}{D_c(K_m + c_\infty)} = -\frac{D_m}{D_c}[B_m]_\infty \quad (15)$$

and $[B_m]_\infty$, the concentration of free mobile buffer in the absence of the source, is defined as $[B_m]_\infty \equiv [B_m]_T K_m/(K_m + c_\infty)$. Fig. 4 compares this near source estimate of the decline in $[Ca^{2+}]_d$ because of the presence of a single mobile buffer to the value predicted by the steady-state rapid buffering approximation in the presence and absence of mobile buffer. The reliability of the near source estimate provided by Eq. 14 depends, of course, on the radius at which $[Ca^{2+}]_d$ is defined. Near the Ca^{2+} channel ($r < 0.1$ μm), Eq. 14 provides a good estimate of the effect of mobile buffer on $[Ca^{2+}]_d$; however, at larger distances ($r > 0.1$ μm) the near source estimate breaks down and Eq. 11 must be used.

Effect of bulk lumenal Ca^{2+} on $[Ca^{2+}]_d$

In the previous sections we considered a hemispherical domain surrounding a Ca^{2+} source of arbitrary amplitude; however, the Ca^{2+} flux through an open intracellular Ca^{2+} channel is presumably related to the driving force for Ca^{2+} and, consequently, the bulk Ca^{2+} concentration on the lumenal side of the endoplasmic or sarcoplasmic reticulum membrane. The steady-state rapid buffering approximation can be used to investigate the effect of bulk lumenal Ca^{2+} on the cytosolic domain Ca^{2+} concentration ($[Ca^{2+}]_d$) by matching cytosolic and lumenal Ca^{2+} profiles. Conservation of Ca^{2+} is an obvious constraint on this match—the source amplitudes must be equal and opposite so that all the Ca^{2+} that leaves the lumen enters the cytosol. A parameter required for the match is the free Ca^{2+} drop over the channel ($\Delta[Ca^{2+}]_d^{drop}$), defined as

$$\Delta[Ca^{2+}]_d^{drop} \equiv [Ca^{2+}]_d^L - [Ca^{2+}]_d^R, \quad (16)$$

where L and R indicate the lumen and cytosol, respectively; and $[Ca^{2+}]_d^L$ and $[Ca^{2+}]_d^R$ are the lumenal and cytosolic domain concentrations. For example, if the flux into the

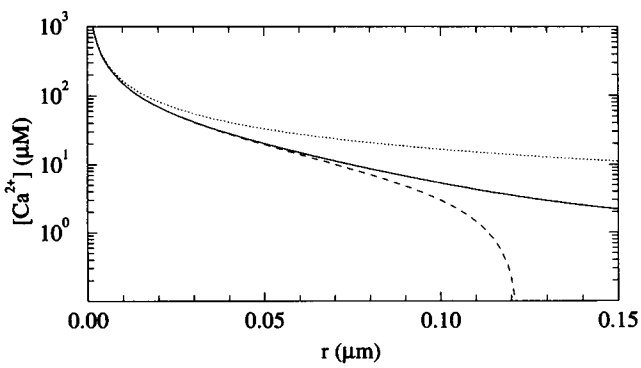

FIGURE 4 For a range of distances (r) near a 0.5 pA Ca^{2+} channel, the near source estimate (*dashed line*) of the effect of mobile buffer on $[Ca^{2+}]_d$ given by Eq. 14 is compared to that calculated using the steady-state rapid buffering approximation, Eq. 10, both with (*solid line*) and without (*dotted line*) mobile buffer. Source amplitude (σ) is 0.5 pA, c_∞ = 0.1 μM, and D_c = 250 $\mu m^2/s$. Parameters for mobile buffer (when included) are $[B_m]_T$ = 50 μM, K_m = 1 μM, and D_m = 75 $\mu m^2/s$, which lead to $\Delta[Ca^{2+}]_d^{app}$ = −13.64 μM using Eq. 15.

cytosol (σ_R) is directly proportional to the local concentration difference between the two sides ($\sigma_R = g\,([Ca^{2+}]_d^L - [Ca^{2+}]_d^R)$), then $\Delta[Ca^{2+}]_d^{drop}$ is σ_R/g. Appendix C details how Eq. 16 and Eq. 9 can be used to obtain the following implicit, analytical expression for $[Ca^{2+}]_d^R$,

$$h_L([Ca^{2+}]_d^R + \Delta[Ca^{2+}]_d^{drop}) + h_R([Ca^{2+}]_d^R) = h_L(c_\infty^L) + h_R(c_\infty^L), \quad (17)$$

where the functions h_L and h_R are defined as,

$$h_i([Ca^{2+}]) \equiv D_c^i[Ca^{2+}] - \sum_j \frac{\Phi_j^i}{K_j^i + [Ca^{2+}]}, \quad (18)$$

and $i = L$ or R. Given a set of physiologically realistic parameters for $\Delta[Ca^{2+}]_d^{drop}$ and lumenal and cytosolic buffers, $[Ca^{2+}]_d^R$ can be found numerically as the root of Eq. 17. This value for $[Ca^{2+}]_d^R$ then determines $[Ca^{2+}]_d^L$ as well as the cytosolic and lumenal profiles (see Appendix C).

Fig. 5 shows the cytosolic (*solid line*) and lumenal (*dotted line*) Ca^{2+} profile near an open intracellular Ca^{2+} channel given the cytosolic domain Ca^{2+} concentration ($[Ca^{2+}]_d^R$) of 37.4 μM (*filled circle*) estimated using Eq. 17. We assume that the free Ca^{2+} drop over the channel ($\Delta[Ca^{2+}]_d^{drop}$) is 15 μM, the lumen has a fivefold higher buffer capacity and dissociation constant than the cytosol ($[B_m]_T^L$ = 250 μM, K_m^L = 5 μM, $[B_m]_T^R$ = 50 μM, K_m^R = 1 μM), the bulk lumenal Ca^{2+} concentration (c_∞^L) is 100 μM, c_∞^R is 0.1 μM, and the source amplitude of the channel is 0.41 pA. Fig. 5 suggests that lumenal depletion domains, like cytosolic Ca^{2+} domains, can be localized by mobile Ca^{2+} buffers and may be of comparable size.

Fig. 6 shows the functional dependence of the cytosolic domain Ca^{2+} concentration ($[Ca^{2+}]_d^R$) on bulk lumenal Ca^{2+} (c_∞^L) predicted by Eq. 17 for various concentrations of lumenal ($[B_m]_T^L$ = 0 or 250 μM) and cytosolic ($[B_m]_T^R$ = 0 or 50 μM) mobile buffer (other parameters as in Fig. 5). In all cases, the cytosolic domain Ca^{2+} concentration is an increasing function of bulk lumenal Ca^{2+}. Fig. 6 also shows that high concentrations of lumenal mobile buffer are associated with elevated $[Ca^{2+}]_d^R$ (compare *short-dashed* and *long-dashed lines*) and, according to Eq. 16, less depleted $[Ca^{2+}]_d^L$. This observation suggests that lumenal mobile buffer may increase cytosolic Ca^{2+} domain concentrations by facilitating the transport of lumenal Ca^{2+} toward the lumenal pore. Given the dissociation constants used in Fig. 6 (K_m^L = 5 μM, K_m^R = 1 μM), the relationship between $[Ca^{2+}]_d^R$ and bulk lumenal Ca^{2+} (c_∞) is nearly linear; however, this is strictly true only in the absence of both lumenal and cytosolic mobile buffers (*dotted line*; see Appendix C).

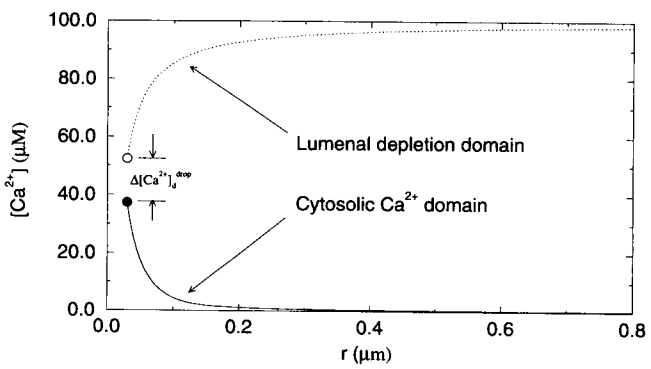

FIGURE 5 Calculation of steady-state Ca^{2+} domain (*solid line*) along with a matching calculation of an ER depletion domain (*dotted line*). Parameters for both cytosol and ER were: $[B_m]_T^L$ = 250 μM, K_m^L = 5 μM, $[B_m]_T^R$ = 50 μM, K_m^R = 1 μM, D_c^i = 250 $\mu m^2/s$, D_m^i = 75 $\mu m^2/s$, c_∞^L = 100 μM, c_∞^R = 0.1 μM, r_0 = 0.03 μm, σ_R = 0.41 pA. Solid dot shows $[Ca^{2+}]_d^R$ = 37.4 μM calculated using Eq. 17, assuming $\Delta[Ca^{2+}]_d^{drop}$ = 15 μM. Open circle shows $[Ca^{2+}]_d^L = [Ca^{2+}]_d^R + \Delta[Ca^{2+}]_d^{drop}$ = 52.4 μM.

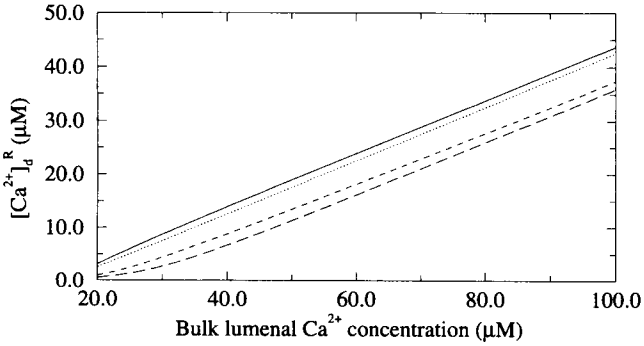

FIGURE 6 Calculation of the cytosolic Ca^{2+} domain concentration ($[Ca^{2+}]_d^R$) as a function of bulk lumenal Ca^{2+} (c_∞^L) using Eq. 17 and various concentrations of lumenal mobile buffer. From top to bottom, $[B_m]_T^L$ and $[B_m]_T^R$ in μM: 250 and 0 (*solid line*), 0 and 0 (*dotted line*), 250 and 50 (*short-dashed line*), 0 and 50 (*long-dashed line*). In all cases, K_m^L = 5 μM and K_m^R = 1 μM. Other parameters: D_c^i = 250 $\mu m^2/s$, D_m^i = 75 $\mu m^2/s$, c_∞^R = 0.1 μM.

CONCLUSION

The steady-state rapid buffering approximation near an open Ca^{2+} channel is a novel analytical result that complements the excess buffer approximation (Neher, 1986) because of the different assumptions made in their derivations (see Appendices A and B). Whereas the excess buffer approximation begins with the full equations for the buffered diffusion of Ca^{2+}, Eqs. 1–3, and assumes that mobile buffers are unsaturable, the steady-state rapid buffering approximation begins with the reduced equation for the transport of Ca^{2+}, Eq. 6. Both results assume hemispherical symmetry and a point source for Ca^{2+} ions. These two approximations are complementary in the sense that they are valid in different parameter regimes, but it is important to note that in some cases neither approximation can be applied (Smith et al., 1996).

When the conditions for the validity of the rapid buffering approximation near a point source for Ca^{2+} ions are met (Smith et al., 1996), the steady-state rapid buffering approximation provides an upper limit on the Ca^{2+} profile during a local Ca^{2+} elevation. It can also be used to relate source amplitude of a local Ca^{2+} elevation to an observed Ca^{2+}-

bound dye profile. Indeed, after being transformed to account for spatial averaging due to the cubic micrometer resolution of confocal microscopy, CaB_e profiles calculated using the steady-state rapid buffering approximation can be directly compared to fluorescence measurements to provide a lower bound on the source amplitude responsible for an observed Ca^{2+}-bound dye profile.

The steady-state rapid buffering approximation is much easier to use than numerically solving for the steady-state Ca^{2+} profile using a finite difference approximation to either the full or reduced equations. In the case of a single mobile buffer, we have derived an explicit analytical expression of the Ca^{2+} concentration as a function of r, Eq. 11. When more than one mobile buffer is present, we have numerically solved for the roots of Eq. 10 for each value of r of interest. Because the left side of Eq. 10 is a monotonically increasing function of physiological Ca^{2+} concentrations, algorithms that numerically solve this equation are easily implemented.

Because the steady-state Ca^{2+} concentration is achieved rapidly near the pore of an open Ca^{2+} channel, Eqs. 10 and 11 provide a good estimate of the effect of mobile buffers and bulk cytosolic Ca^{2+} on the domain Ca^{2+} concentration ($[Ca^{2+}]_d$) when the rapid buffering approximation is valid. Beginning with Eq. 11, we also derived an even simpler expression, Eq. 14, which relates changes in $[Ca^{2+}]_d$ caused by mobile Ca^{2+} buffer to the unbound mobile buffer concentration distant from the source ($[B_m]_\infty$). This near source estimate of the change in $[Ca^{2+}]_d$ due to a mobile buffer generalizes to

$$\Delta[Ca^{2+}]_d^{app} \equiv -\frac{1}{D_c}\sum_j D_j[B_j]_\infty \tag{19}$$

when multiple buffers are present.

Assuming a simple relationship between the cytosolic and lumenal Ca^{2+} domain concentrations, an expression for the dependence of $[Ca^{2+}]_d$ on bulk lumenal Ca^{2+} was derived. Although the procedure used to match lumenal and cytosolic Ca^{2+} profiles is very simplistic, Eq. 17 suggests the possibility of incorporating the steady-state rapid buffering approximation into realistic models of the IP_3R and RyR that include the effect of domain Ca^{2+} and the possible regulation of these intracellular Ca^{2+} channels by lumenal Ca^{2+} through a cytosolic Ca^{2+} binding site. Work along these lines is currently in progress.

APPENDIX A: DERIVATION OF THE EXCESS BUFFER APPROXIMATION

The excess buffer approximation (Neher, 1986) is derived from Eqs. 1–3 by assuming mobile buffer is unsaturable ($[B_m] \approx [B_m]_T$, $[B_m]$ and $[CaB_m]$ are assumed constant in space and time), writing the Laplacian operator in spherical polar coordinates, that is,

$$\nabla^2 = \frac{\partial^2}{\partial r^2} + \frac{2}{r}\frac{\partial}{\partial r}, \tag{20}$$

and setting $\partial[Ca^{2+}]/\partial t = 0$. This leads to (Neher, 1986)

$$\frac{d^2[Ca^{2+}]}{dr^2} = -\frac{2}{r}\frac{d[Ca^{2+}]}{dr} + \frac{[Ca^{2+}] - c_\infty}{\lambda^2} \quad (r > 0) \tag{21}$$

where $\lambda^2 = D_c/k_m^+[B_m]_T$. A solution to Eq. 21 is given by

$$[Ca^{2+}] = A_1 r^{-1} e^{-r/\lambda} + c_\infty \tag{22}$$

and can be derived by the substitution $\mu = r([Ca^{2+}] - c_\infty)$. To satisfy the boundary condition given by the bulk Ca^{2+} concentration far from the channel (c_∞), that is,

$$\lim_{r\to\infty}[Ca^{2+}] = c_\infty \tag{23}$$

we require λ to be positive, that is, $\lambda = \sqrt{D_c/k_m^+[B_m]_T}$. A radiative boundary condition near the channel is given by

$$\lim_{r\to 0}\left[-2\pi r^2 D_c \frac{d[Ca^{2+}]}{dr}\right] = \sigma \tag{24}$$

where the quantity in the brackets is the flux at radius r and σ is source amplitude of the ion channel. This second boundary condition leads to $A_1 = \sigma/2\pi D_c$, which upon substitution into Eq. 22 gives Eq. 5.

APPENDIX B: DERIVATION OF THE STEADY-STATE RAPID BUFFERING APPROXIMATION

The steady-state rapid buffering approximation near an open Ca^{2+} channel, Eq. 9, is derived by dividing Eq. 7 by $d[Ca^{2+}]/dr$ to give (Polyanin and Zaitsev, 1995)

$$\left(\frac{d[Ca^{2+}]}{dr}\right)^{-1}\frac{d}{dr}\left(\frac{d[Ca^{2+}]}{dr}\right) = -\frac{2}{r} + f([Ca^{2+}])\frac{d[Ca^{2+}]}{dr} \quad (r > 0) \tag{25}$$

and then multiplying by dr to obtain

$$\left(\frac{d[Ca^{2+}]}{dr}\right)^{-1} d\left(\frac{d[Ca^{2+}]}{dr}\right) = -\frac{2}{r}dr + f([Ca^{2+}])d[Ca^{2+}]. \tag{26}$$

The above expression is an exact differential equation that can be integrated to give

$$\ln\left|\frac{d[Ca^{2+}]}{dr}\right| = -2\ln r + F([Ca^{2+}]) + \ln C_1 \tag{27}$$

where

$$F([Ca^{2+}]) = \int f([Ca^{2+}])d[Ca^{2+}]. \tag{28}$$

Using the definition of γ_j in Eq. 6 and $\Phi_j = D_j[B_j]_T K_j$ we have the identity

$$\gamma_j D_j = \Phi_j(K_j + [Ca^{2+}])^{-2}, \tag{29}$$

which can be used to rewrite Eq. 8 to give

$$f([Ca^{2+}]) = 2\left[\sum_j \Phi_j\,(K_j + [Ca^{2+}])^{-3}\right] \Big/ \left[D_c + \sum_j \Phi_j\,(K_j + [Ca^{2+}])^{-2}\right]. \quad (30)$$

Because

$$d[\Phi_j(K_j + [Ca^{2+}])^{-2}] = -2\Phi_j(K_j + [Ca^{2+}])^{-3}\,d[Ca^{2+}], \quad (31)$$

it follows that

$$d\left[D_c + \sum_j \Phi_j\,(K_j + [Ca^{2+}])^{-2}\right] = -2\sum_j \Phi_j(K_j + [Ca^{2+}])^{-3}\,d[Ca^{2+}], \quad (32)$$

and the integral $F([Ca^{2+}])$ is calculated to be

$$F([Ca^{2+}]) = -\ln\left[D_c + \sum_j \Phi_j(K_j + [Ca^{2+}])^{-2}\right]. \quad (33)$$

Exponentiating both sides of Eq. 27 thus leads to

$$\left|\frac{d[Ca^{2+}]}{dr}\right| = \frac{C_1}{r^2(D_c + \sum_j \gamma_j D_j)} \quad (34)$$

where $C_1 \geq 0$. We can drop the absolute value sign and remove this restriction on C_1, remembering that its sign, which can now be positive or negative, determines the sign of $d[Ca^{2+}]/dr$. Performing separation of variables and integrating Eq. 34 gives

$$\int\left[D_c + \sum_j \gamma_j D_j\right] d[Ca^{2+}] = C_1 \int \frac{dr}{r^2} + C_2, \quad (35)$$

from which Eq. 9 follows.

By taking the limit of Eq. 9 as r goes to infinity, one finds that the boundary condition given by the bulk Ca^{2+} concentration (c_∞) leads to

$$C_2 = D_c c_\infty - \sum_j \frac{\Phi_j}{K_j + c_\infty}. \quad (36)$$

A radiative boundary condition near the channel is given by (Wagner and Keizer, 1994)

$$\lim_{r\to 0}\left\{-2\pi r^2\beta\left[D_c + \sum_j \gamma_j D_j\right]\frac{d[Ca^{2+}]}{dr}\right\} = \beta\sigma, \quad (37)$$

which, together with Eq. 34, leads to $C_1 = -\sigma/2\pi$. Substituting these values for the integration constants into Eq. 9 gives Eq. 10.

In the case of only one mobile buffer, the quadratic formula can be used to obtain Eq. 11 from Eq. 10. The question of which branch of the square root is physical can be resolved by considering the limit of Eq. 11 as r goes to infinity,

$$\lim_{r\to\infty}[Ca^{2+}] = (-D_c K_m + C_2 \pm \sqrt{(D_c K_m + C_2)^2 + 4D_c\Phi_m})/2D_c. \quad (38)$$

Because C_2 is given by Eq. 36 we can substitute and rearrange the resulting expression to give,

$$\lim_{r\to\infty}[Ca^{2+}] = \left(-D_c K_m + D_c c_\infty - \frac{\Phi_m}{c_\infty + K_m} \pm \left|D_c K_m + D_c c_\infty + \frac{\Phi_m}{c_\infty + K_m}\right|\right)\Big/ 2D_c \quad (39)$$

where the quantity within the absolute value signs is positive. The positive branch of the square root gives the correct result, $\lim_{r\to\infty}[Ca^{2+}] = c_\infty$, whereas the negative branch is not physical as it leads to $\lim_{r\to\infty}[Ca^{2+}] \leq 0$.

APPENDIX C: MATCHING CYTOSOLIC AND LUMENAL Ca^{2+} PROFILES

To illustrate the matching procedure used to derive Eq. 17 we will first consider the simple case where mobile buffers are absent and the cytosolic and lumenal Ca^{2+} profiles near an open intracellular Ca^{2+} channel are given on two abutted hemispherical domains by steady states of the radial diffusion equation (Carslaw and Jaeger, 1959),

$$0 = \frac{\partial c^i}{\partial t} = \frac{D_i}{r^2}\frac{\partial}{\partial r}\left(r^2\frac{\partial c^i}{\partial r}\right) \quad (40)$$

where the index $i = L, R$ again indicates the lumenal or cytosolic side. Solutions to Eq. 40 are given by

$$c_i = \frac{r_0([Ca^{2+}]_d^i - c_\infty^i)}{r} + c_\infty^i \quad (r_0 \leq r < \infty) \quad (41)$$

where c_∞^i is the bulk Ca^{2+} concentration on each side, r_0 is the first radius at which the solution is defined, and $[Ca^{2+}]_d^i$ are domain Ca^{2+} concentrations yet to be determined. At steady state the flux (σ_i) over any hemisphere of radius r is given by

$$\sigma_i \equiv -2\pi r^2 D_i\frac{dc_i}{dr} = 2\pi r_0 D_i([Ca^{2+}]_d^i - c_\infty^i) \quad (42)$$

Conservation of Ca^{2+} allows us to relate the domain Ca^{2+} concentrations on each side through $\sigma_L = -\sigma_R$, that is,

$$D_L([Ca^{2+}]_d^L - c_\infty^L) = -D_R([Ca^{2+}]_d^R - c_\infty^R). \quad (43)$$

The definition of $\Delta[Ca^{2+}]_d^{drop}$ (Eq. 16) relates $[Ca^{2+}]_d^R$ and $[Ca^{2+}]_d^L$ and can be solved simultaneously with Eq. 43 to give the following expression for the domain Ca^{2+} concentration ($[Ca^{2+}]_d^R$)

$$[Ca^{2+}]_d^R = \frac{D_R c_\infty^R + D_L c_\infty^L}{D_R + D_L} - \frac{D_L}{D_R + D_L}\Delta[Ca^{2+}]_d^{drop}. \quad (44)$$

$[Ca^{2+}]_d^L$ is then given by $[Ca^{2+}]_d^L = [Ca^{2+}]_d^R + \Delta[Ca^{2+}]_d^{drop}$, and the Ca^{2+} profile is found by substituting the above expression into Eq. 41.

To include the effect of mobile buffers in this analysis, we begin with two Ca^{2+} profiles that are steady states to the rapid buffering approximation and choose the integration constants in Eq. 9 so that 1) the boundary condition given by the bulk Ca^{2+} concentration ($C_2^i = h_i\,(c_\infty^i)$, h_i as defined

in Eq. 18) is satisfied, and 2) the Ca^{2+} concentration at $r = r_0$ is given by $[Ca^{2+}]_d^i$, that is,

$$C_1^i = -r_0(h_i([Ca^{2+}]_d^i) - h_i(c_\infty^i)). \quad (45)$$

With C_1^i and C_2^i specified in this manner, the Ca^{2+} profile is given by

$$h_i([Ca^{2+}]^i) = \frac{r_0}{r}(h_i([Ca^{2+}]_d^i) - h_i(c_\infty^i)) + h_i(c_\infty^i) \quad (46)$$

$$(r_0 \le r < \infty).$$

Because Eq. 46 is now in the form of Eq. 41, the matching procedure of the previous section can be used to determine $[Ca^{2+}]_d^L$ and $[Ca^{2+}]_d^R$. Eqs. 37 and 34 together give $\sigma_i = -2\pi C_1^i$, so upon setting the fluxes equal and opposite ($\sigma_L = -\sigma_R$) we have $C_1^L = -C_1^R$, that is,

$$h_L([Ca^{2+}]_d^L) - h_L(c_\infty^L) = -(h_R([Ca^{2+}]_d^R) - h_R(c_\infty^R)), \quad (47)$$

which is written in a form similar to Eq. 43. Using Eq. 16 to rewrite $[Ca^{2+}]_d^L$ gives Eq. 17. For a given $\Delta[Ca^{2+}]_d^{drop}$, $[Ca^{2+}]_d^R$ can be found numerically as the root of Eq. 17, and these values then give $[Ca^{2+}]_d^L$. The domain Ca^{2+} concentrations can then be used in Eq. 46 to calculate the corresponding lumenal and cytosolic Ca^{2+} profiles.

This work was supported in part by funds from National Institutes of Health grant R01 RR 10081-01A1 and National Science Foundation grants BIR 92-14381 and BIR 93-00799 to Joel Keizer, and the Agricultural Experiment Station of University of California, Davis. GDS gratefully acknowledges fellowship support from the Biophysics Graduate Group at University of California Davis and the Jastro-Shields Foundation, and conversations with Joel Keizer.

REFERENCES

Adler, E. M., G. J. Augustine, S. N. Duffy, and M. P. Charlton. 1991. Alien intracellular calcium chelators attenuate neurotransmitter release at the squid giant synapse. *J. Neurosci.* 11:1496–1507.

Allbritton, N. L., T. Meyer, and L. Stryer. 1992. Range of messenger action of Ca^{2+} ion and inositol 1,4,5-trisphosphate. *Science.* 258:1812–1815.

Bezprozvanny, I., and B. E. Ehrlich. 1994. IP_3-gated Ca^{2+} channels from cerebellum: conduction properties for divalent cations and regulation by intralumenal Ca^{2+}. *J. Gen. Physiol.* 104:821–856.

Bezprozvanny, I., and B. E. Ehrlich. 1995. The inositol 1,4,5-trisphosphate (IP_3) receptor. *J. Membr. Biol.* 145:205–216.

Cannell, M. B., H. Cheng, and W. J. Lederer. 1994. Spatial non-uniformities in $[Ca^{2+}]_i$ during excitation-contraction coupling in cardiac myocytes. *Biophys. J.* 67:1942–1956.

Cannell, M. B., H. Cheng, and W. J. Lederer. 1995. The control of Ca^{2+} release in heart muscle. *Science.* 268:1045–1049.

Carslaw, H. S., and J. C. Jaeger. 1959. Conduction of Heat in Solids, 2nd ed. Clarendon Press, Oxford.

Cheng, H., W. J. Lederer, and M. B. Cannell. 1993. Calcium sparks: elementary events underlying excitation-contraction coupling in heart muscle. *Science.* 262:740–744.

Clapham, D. E. 1995. Calcium signaling. *Cell.* 80:259–268.

DeFelice, L. J. 1993. Molecular and biophysical view of the Ca^{2+} channel: a hypothesis regarding oligomeric structure, channel clustering, and macroscopic current. *J. Membr. Biol.* 133:191–202.

Heinemann, C., R. H. Chow, E. Neher, and R. Zucker. 1994. Kinetics of the secretory response in bovine chromaffin cells following flash photolysis of caged Ca^{2+}. *Biophys. J.* 67:2546–2557.

Horne, J. H., and T. Meyer. 1995. Luminal calcium regulates the inositol trisphosphate receptor of rat basophilic leukemia cells at a cytosolic site. *Biochemistry* 34:12738–12746.

Jafri, M. S., and J. Keizer. 1995. On the roles of Ca^{2+} diffusion, Ca^{2+} buffers, and the endoplasmic reticulum in IP_3-induced Ca^{2+} waves. *Biophys. J.* 69:2139–2153.

Li, Y.-X., J. Rinzel, L. Vergara, and S. Stojilković. Spontaneous electrical and calcium oscillations in unstimulated pituitary gonadotrophs. *Biophys. J.* 69:785–795.

Mazzanti, M., L. J. DeFelice, and Y.-M. Liu. 1991. Gating of L-type Ca^{2+} channels in embryonic chick ventricle cells: dependence on voltage, current and channel density. *J. Physiol.* 443:307–334.

Monck, J. R., I. M. Robinson, A. L. Escobar, J. L. Vergara, and J. M. Fernandez. 1994. Pulsed laser imaging of rapid Ca^{2+} gradients in excitable cells. *Biophys. J.* 67:505–514.

Neher, E. 1986. Concentration profiles of intracellular Ca^{2+} in the presence of diffusible chelator. *Exp. Brain Res.* 14:80–96.

Nelson, M. T., H. Cheng, M. Rubart, L. F. Santana, A. D. Bonev, H. J. Knot, and W. J. Lederer. 1995. Relaxation of arterial smooth muscle by calcium sparks. *Science.* 270:633–637.

Parker, I., and Y. Yao. 1996. Ca^{2+} transients associated with openings of inositol trisphosphate-gated channels in *Xenopus* oocytes. *J. Physiol. (Lond.).* 491:663–668.

Polyanin, A. D., and V. F. Zaitsev. 1995. Handbook of Exact Solution for Ordinary Differential Equations. CRC Press, New York.

Risso, S., and L. J. DeFelice. 1993. Ca^{2+} channel kinetics during the spontaneous heart beat in embryonic chick ventricle cells. *Biophys. J.* 65:1006–1018.

Rizzuto, R., M. Brini, M. Murgia, and T. Pozzan. 1996. Microdomains with high Ca^{2+} close to IP_3-sensitive channels that are sensed by neighboring mitochondria. *Science.* 262:744–747.

Roberts, W. M. 1993. Spatial Ca^{2+} buffering in saccular hair cells. *Nature.* 363:74–76.

Roberts, W. M. 1994. Localization of Ca^{2+} signals by a mobile Ca^{2+} buffer in frog saccular hair cells. *J. Neurosci.* 14:3246–3262.

Sherman, A., J. Keizer, and J. Rinzel. 1990. Domain theory for Ca^{2+} inactivation of open Ca^{2+} channels. *Biophys. J.* 58:985–995.

Silver, R. A., A. G. Lamb, and S. R. Bolsover. 1990. Calcium hotspots caused by L-channel clustering promote morphological changes in neuronal growth cones. *Nature.* 343:751–754.

Simon, S. M., and R. Llinás. 1985. Compartmentalization of the submembrane Ca^{2+} activity during Ca^{2+} influx and its significance in transmitter release. *Biophys. J.* 48:485–498.

Smith, G. D., J. Wagner, and J. Keizer. 1996. Validity of the rapid buffering approximation near a point source of calcium ions. *Biophys. J.* 70:2527–2539.

Stern, M. D. 1992. Buffering of Ca^{2+} in the vicinity of a channel pore. *Cell Calcium.* 13:183–192.

Swillens, S., L. Combettes, and P. Champeil. 1994. Transient inositol 1,4,5-trisphosphate-induced Ca^{2+} release: A model based on regulatory Ca^{2+}-binding sites along the permeation pathway. *Proc. Natl. Acad. Sci.* 91:10074–10078.

Thorn, P., A. Lawrie, P. Smith, D. Gallagher, and O. Petersen. 1993. Local and global cytosolic Ca^{2+} oscillations in exocrine cells evoked by agonists and inositol trisphosphate. *Cell.* 74:661–668.

Tripathy, A., and G. Meissner. 1996. Sarcoplasmic reticulum lumenal Ca^{2+} has access to cytosolic activation and inactivation sites of skeletal muscle Ca^{2+} release channel. *Biophys. J.* 70:2600–2615.

Tucker, T., and R. Fettiplace. 1995. Confocal imaging of calcium microdomains and calcium extrusion in turtle hair cells. *Neuron.* 15:1323–1335.

Wagner, J., and J. Keizer. 1994. Effects of rapid buffers on Ca^{2+} diffusion and Ca^{2+} oscillations. *Biophys. J.* 67:447–456.

Yao, Y., J. Choi, and I. Parker. 1995. Quantal puffs of intracellular Ca^{2+} evoked by IP_3 in *Xenopus* oocytes. *J. Physiol. (Lond.).* 482:533–553.

Zhou, Z. A., and E. Neher. 1993. Mobile and immobile Ca^{2+} buffers in bovine adrenal chromaffin cells. *J. Physiol. (Lond.).* 469:245–273.

Zucker, R. S., and A. L. Fogelson. 1986. Relationship between transmitter release and presynaptic calcium influx when calcium enters through discrete channels. *Proc. Natl. Acad. Sci.* 83:3032–3036.

Zweifach, A. Z., and R. S. Lewis. 1995. Rapid inactivation of depletion-activated Ca^{2+} current (I_{crac}) due to local Ca^{2+} feedback. *J. Gen. Physiol.* 105:209–206.